Supplementary Information

An autocatalytic multi-component DNAzyme nanomachine for tumor-specific photothermal therapy sensitization in pancreatic cancer

Jiaqi Yan[1,2,5,6,7], Xiaodong Ma[5,6,7], Danna Liang[3,7], Meixin Ran[1,2,5,6,7], Dongdong Zheng[4], Xiaodong Chen[1,2], Shichong Zhou[4], Weijian Sun[3], Xian Shen[1,2]*, Hongbo Zhang[1,2,5,6]**

1 Joint Centre of Translational Medicine, Wenzhou Key Laboratory of Interdiscipline and Translational Medicine, the First Affiliated Hospital of Wenzhou Medical University, Wenzhou, China

2 Department of General Surgery, The First Affiliated Hospital of Wenzhou Medical University, Wenzhou, Zhejiang Province, China

3 Department of Gastrointestinal Surgery, The Second Affiliated Hospital and Yuying Children's Hospital of Wenzhou Medical University, Wenzhou, Zhejiang, 325027, China

4 Department of Ultrasound, Fudan University Shanghai Cancer Center, Shanghai, 200032, PR China

5 Pharmaceutical Sciences Laboratory, Faculty of Science and Engineering, Åbo Akademi University, Turku, Finland

6 Turku Bioscience Centre, University of Turku and Åbo Akademi University, Turku, Finland

7 These authors contributed equally: Jiaqi Yan, Xiaodong Ma, Danna Liang, Meixin Ran

*Corresponding Author E-mail:

Hongbo Zhang : hongbo.zhang@abo.fi ; XianShen : shenxian@wmu.edu.cn; Weijian Sun: fame198288@126.com

Supplementary Table S1. Drug loading for IR780

Input of IR780 (mg)	**2**	**4**	**8**	**10**
IR780 in the bottom after centrifuge (mg)	**0**	**0.008**	**0.808**	**2.020**
Loading efficiency	**100%**	**99.800%**	**89.900%**	**79.800%**
Loading content	**7.40%**	**13.70%**	**22.30%**	**24.10%**

Supplementary Table S2. Drug loading for Curcumin.

Input of Curcumin (mg)	0.5	1	2	3
Curcumin in the bottom after centrifuge (mg)	0.000	0.012	0.051	0.935
Loading efficiency	100%	98.800%	97.450%	68.833%
Loading content	1.960%	3.801%	7.366%	7.629%

Supplementary Table S3

Viability of PANC-1 cells under different concentration of IR780 With 2μg/mL Curcumin, within 50 mg DSPE-PEG-RGD system.

IR780 concentration (μg/mL)						
With 2 μg/mL Curcumin	0	0.5	1	2	4	8
Viability of PANC-1 cells Data are represented as mean ± SD (n = 3).	82.25±3.58	82.26±3.58	69.12±3.44	44.08±6.64	31.37±2.88	32.31±1.06

Supplementary Table S4

Coefficient of drug interaction (CDI) under different concentration of IR780 With 2μg/mL Curcumin

IR780 concentration (μg/mL)	0.5	1	2	4	8
Coefficient of drug interaction (CDI)	0.81733302	0.88390041	0.69443924	0.52012281	0.72445786

Supplementary Table S5

Stability studies for the $^{R}M_{(I+C)}@CaP_{(p)}$ Nano systems at refrigerator and accelerated temperature conditions.

Storage temperature	4℃				40℃			
Time (months)	Initial	1	2	3	Initial	1	2	3
Particle size (nm)	99.5 ± 10.6	100.4 ± 15.7	101.5 ± 9.7	105.3 ± 11.2	101.3. ± 9.2 (ns)	103.4 ± 7.9 (ns)	104.6 ± 8.6 (ns)	105.8 ± 6.6 (ns)
PDI	0.12 ± 0.07	0.21 ± 0.05	0.19 ± 0.11	0.20 ± 0.12	0.16 ± 0.07 (ns)	0.12 ± 0.08 (ns)	0.19 ± 0.03 (ns)	0.21 ± 0.04 (ns)
Zeta potential (mV)	-2.53 ± 0.5	-3.1 ± 1.5	-3.6 ± 1.5	-4.2 ± 2.1	-2.2 ± 0.12 (ns)	-1.1 ± 1.3 (ns)	-1.5 ± 2.3 (ns)	-0.4 ± 0.8 (ns)

Supplementary Table S6. The sequences of DNA oligonucleotides

Name	**No. Sequence (5'→3')**
Target miRNA-21	UAGCUUAUCAGACUGAUGUUGA
Substrate HSP70 mRNA	GCCTTTCCAAGATTGCTGTTT **(3' Inverted dT)**
Left partzyme	TCAACATCAGTGAGACGAATGGAAAG **(3' Inverted dT)**
Right partzyme	CAGCAATTCTCAGCCTGATAAGCTA **(3' Inverted dT)**
Mutated left partzyme	TCAACATCAGTGAGACGAATGCTTTG **(3' Inverted dT)**
Mutated right partzyme	CAGCTTAACTCAGCCTGATAAGCTA **(3' Inverted dT)**

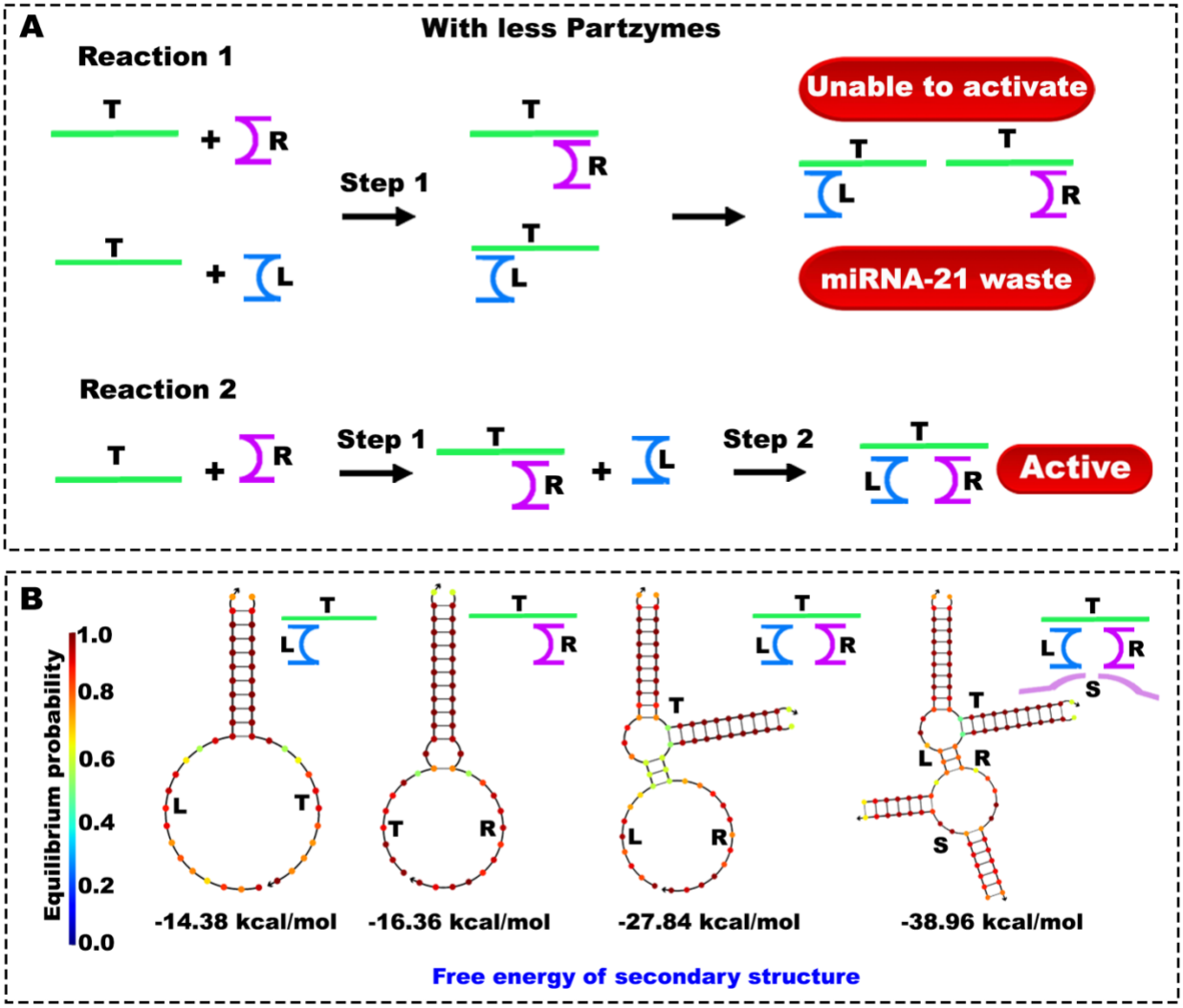

Supplementary Figure 1. The self-building of MNAzyme consists of two processes, T and R would achieve the first conjugation, and then L would combine with T-R complex to realize the second step of MNAzyme construction.

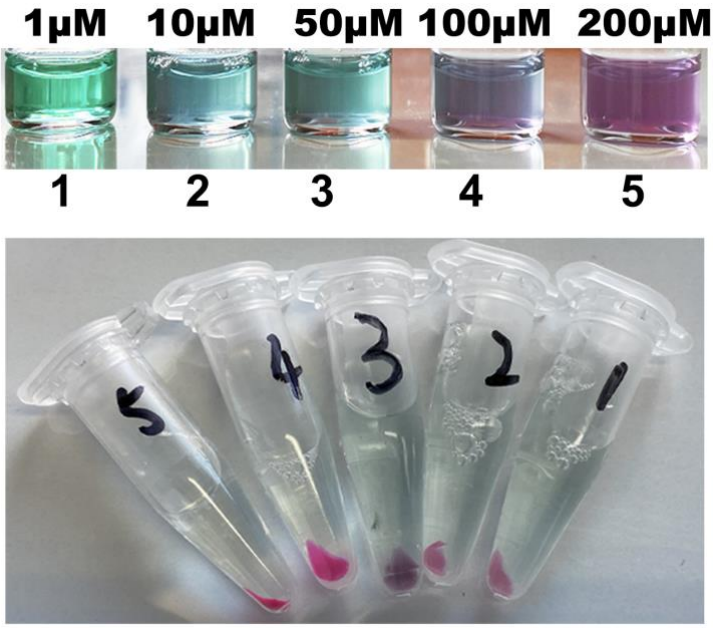

Supplementary Figure 2. Partzyme loading test. Left and right Partzymes were labeled with Cy3 and mixed with 1 mL $^{R}M_{(I+C)}$ solution to form different concentrations of each Partzyme (1μM, 10μM, 50μM, 100μM, 200μM). After calcium phosphate mineralization, we found that all Partzymes were centrifuged to the bottom of the tube (even the content was as high as 200μM), and there was no leakage of Partzyme after several cleaning by Milli-Q water.

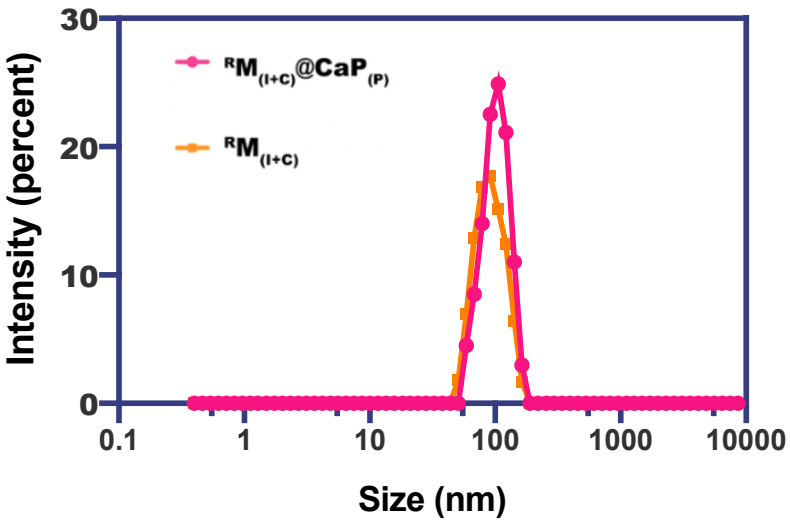

Supplementary Figure 3. The particle size analysis. The particle size analysis revealed the $^{R}M_{(I+C)}$ possessed similar average diameter with $^{R}M_{(I+C)}@CaP_{(p)}$, at around 100 ± 15 nm. (Repeat 3 independent experiments, with similar results). Source data are provided as a Source Data file.

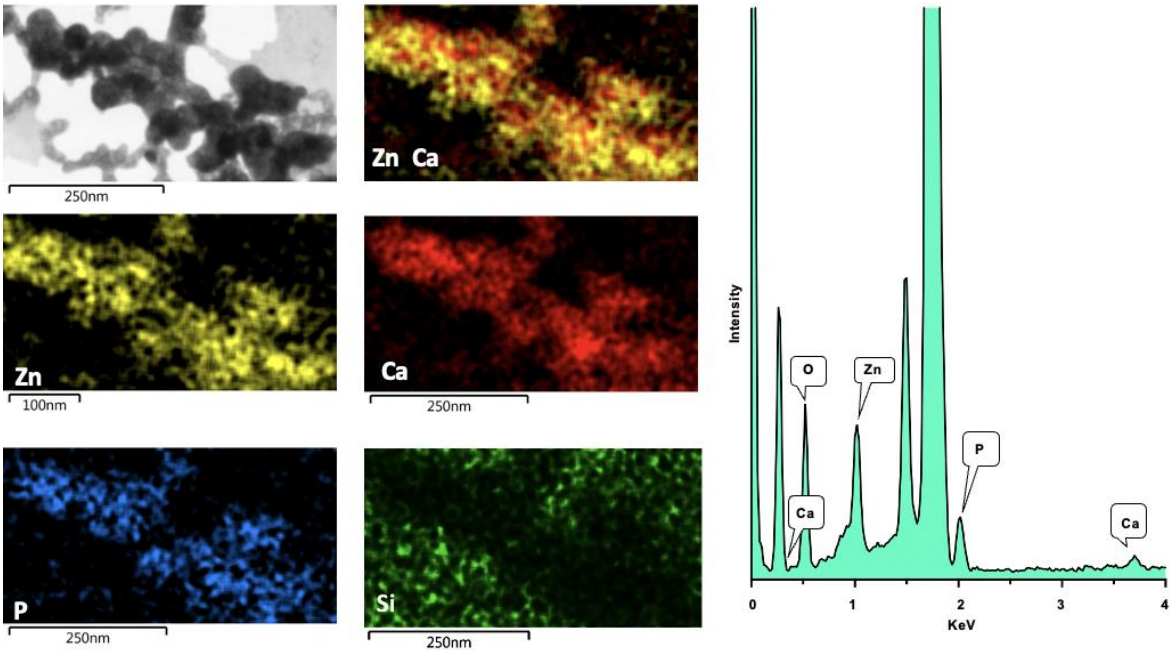

Supplementary Figure 4. Elements mapping for the $^{R}M_{(I+C)}@CaP_{(P)}$ NPs. (Repeat 3 independent experiments, with similar results).

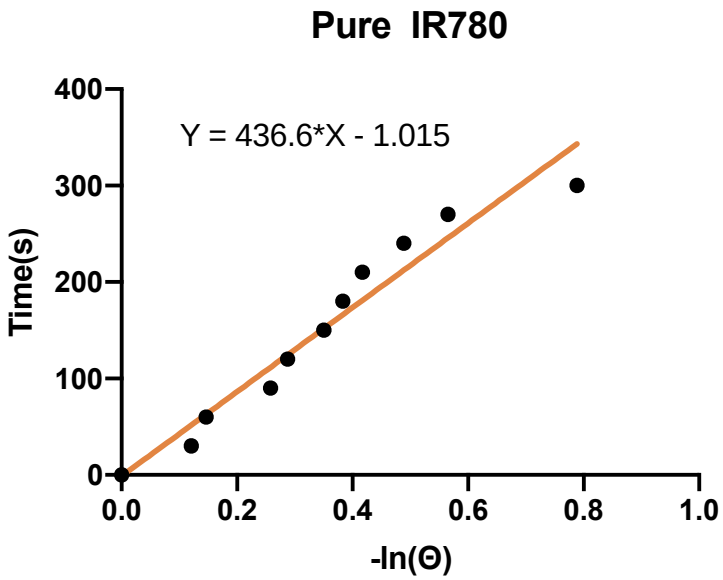

Supplementary Figure 5. The photothermal conversion efficiency of pure drug. (Repeat 3 independent experiments, with similar results) Source data are provided as a Source Data file.

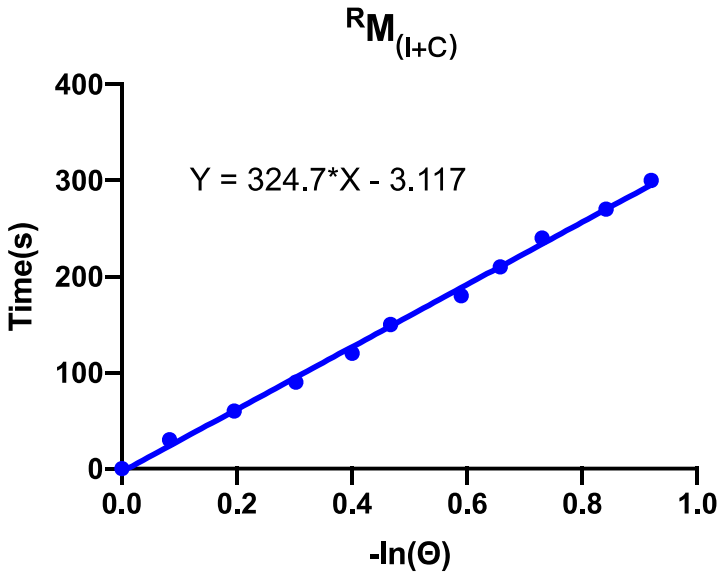

Supplementary Figure 6. the (η) of $^{R}M_{(I+C)}$. (Repeat 3 independent experiments, with similar results) Source data are provided as a Source Data file.

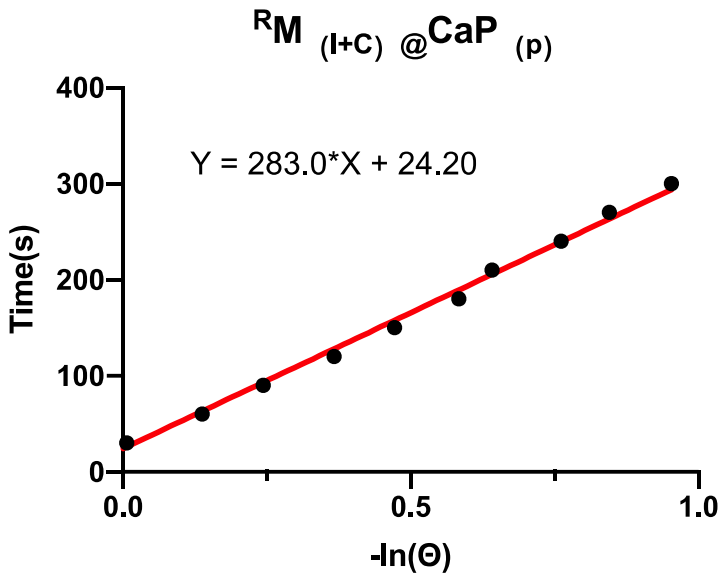

Supplementary Figure 7. the η of IR780 within $^{R}M_{(I+C)}@CaP_{(p)}$ NPs. (Repeat 3 independent experiments, with similar results) Source data are provided as a Source Data file.

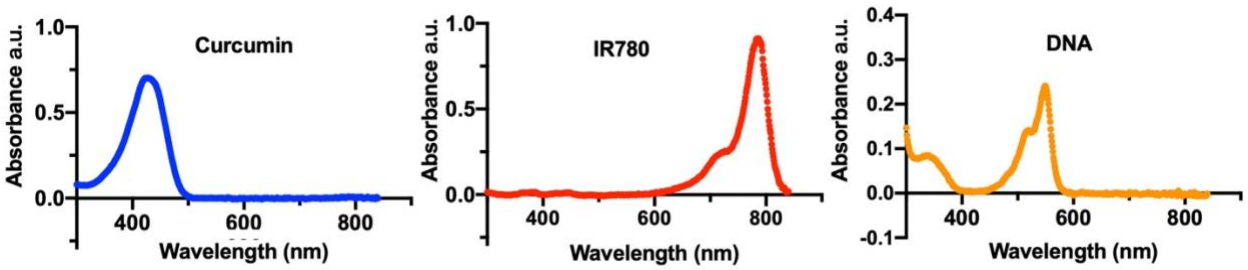

Supplementary Figure 8. UV–Visible spectroscopy for curcumin, IR780 and DNA at 780nm, 425nm and 560nm respectively. Source data are provided as a Source Data file.

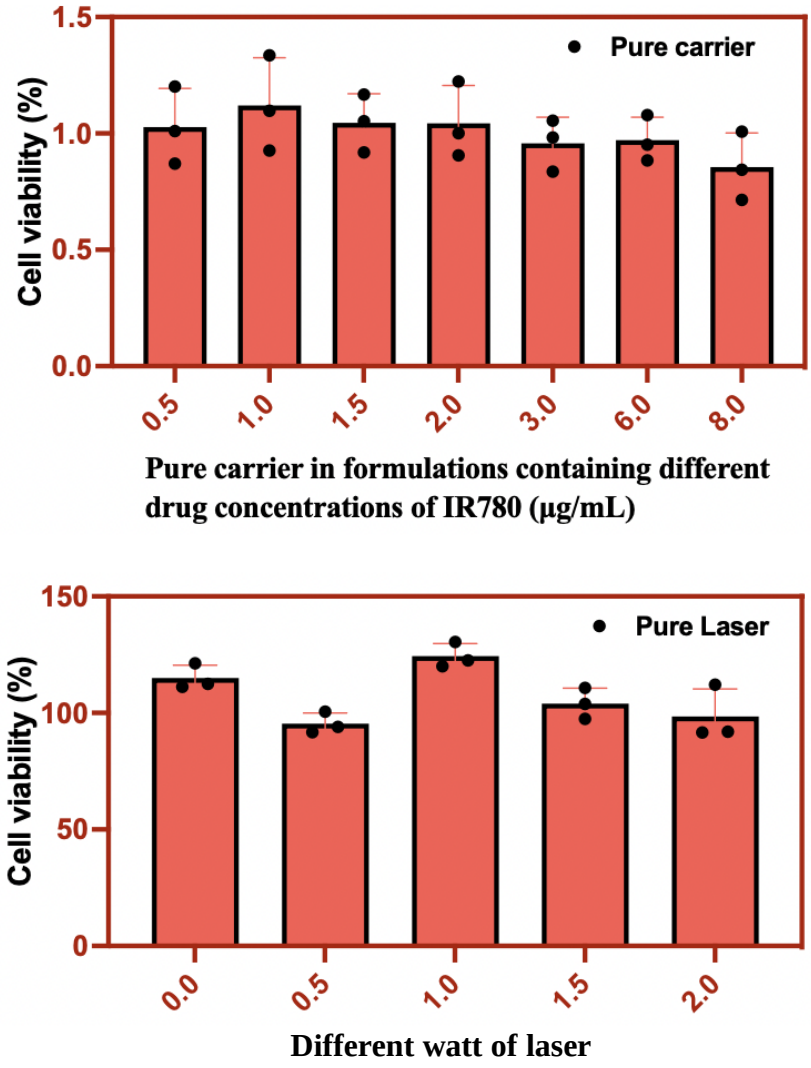

Supplementary Figure 9. The toxicity of pure nanocarrier and laser to normal human dermal fibroblasts NFDH cell line. Pure laser did not inhibit the growth of healthy cells. Source data are provided as a Source Data file. (n = 3 independent experiments and the data are presented as mean values ± SD)

a b

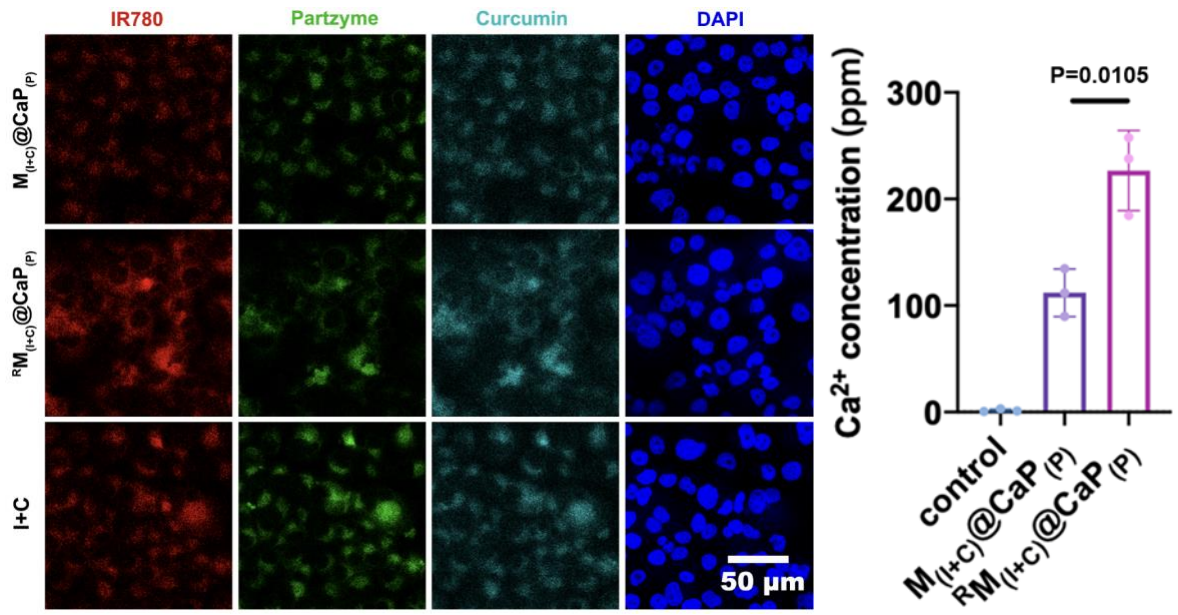

Supplementary Figure 10. The uptake content of each therapeutic agents in PANC-1 cells and the Ca^{2+} concentration. (a)In the case of PANC-1 cells, the results revealed that the uptake content of each therapeutic agents gradually increased along with the extension of 1h. (n = 3 independent experiments, with similar results) (b) The Ca^{2+} concentration detected by ICP-OES. (n = 3 independent experiments and the data are presented as mean values ± SD) All statistics were calculated using two-tailed paired t-test. Source data are provided as a Source Data file.

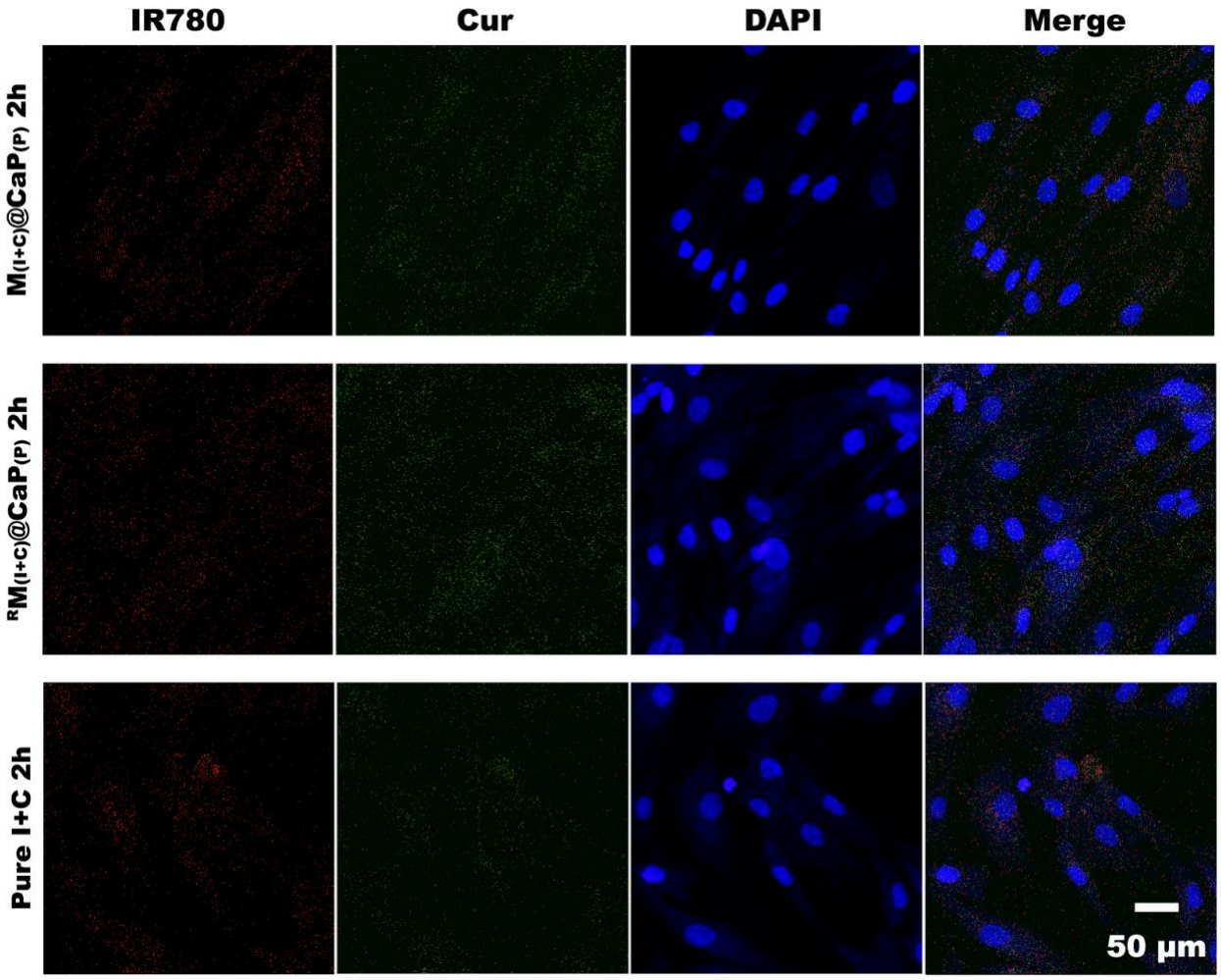

Supplementary Figure 11. Cell uptake for pure drug, $M_{(I+C)}@CaP_{(p)}$ and $^{R}M_{(I+C)}@CaP_{(p)}$ groups in NHDF cells. For NHDF cells, pure drug, $M_{(I+C)}@CaP_{(p)}$ and $^{R}M_{(I+C)}@CaP_{(p)}$ groups all showed negligible uptake after 1h treatment. (n = 3 independent experiments, with similar results)

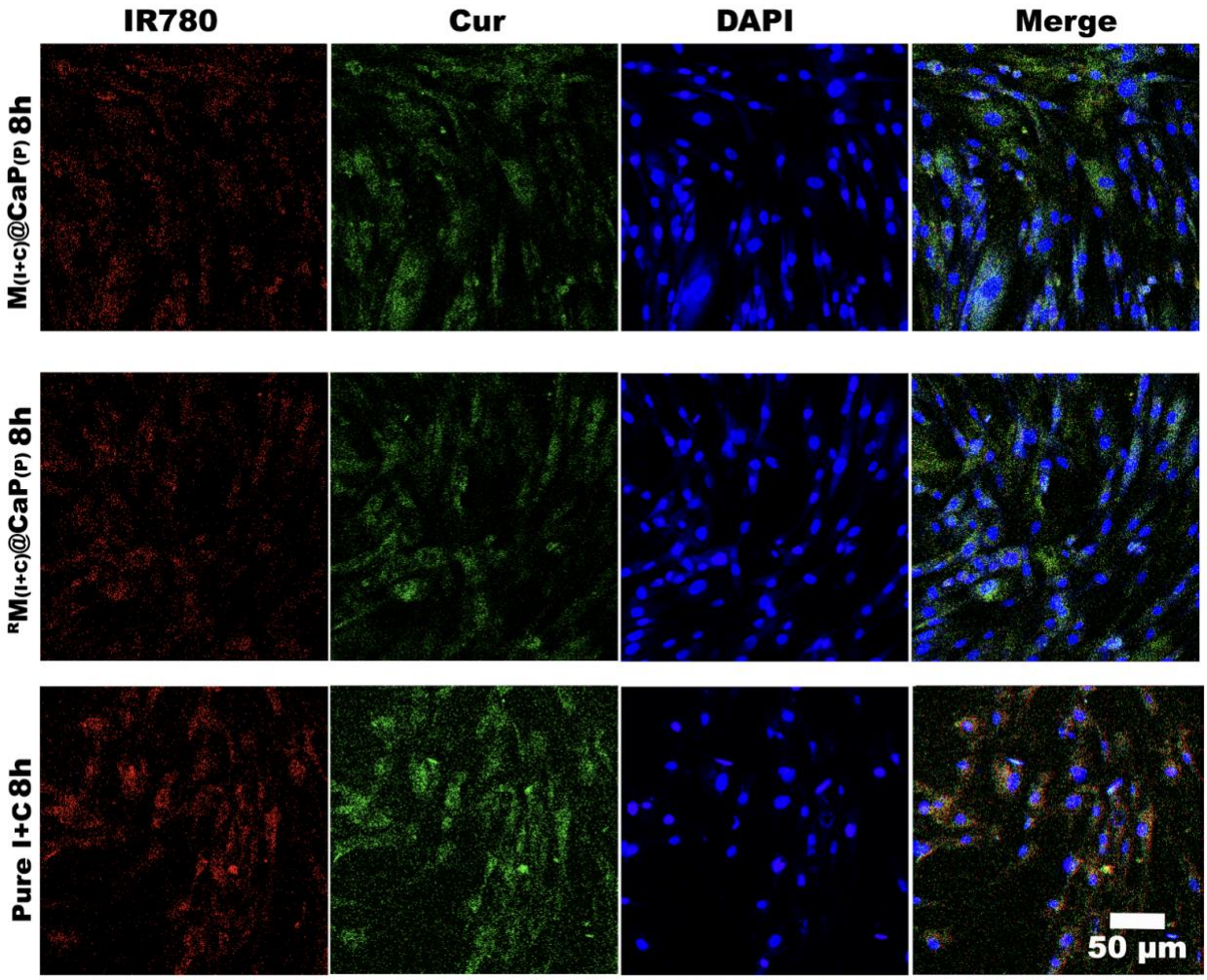

Supplementary Figure 12. The cell uptake of pure drug, $M_{(I+C)}@CaP_{(p)}$ and $^{R}M_{(I+C)}@CaP_{(p)}$ groups by healthy control cell line NHDF. (n = 3 independent experiments, with similar results)

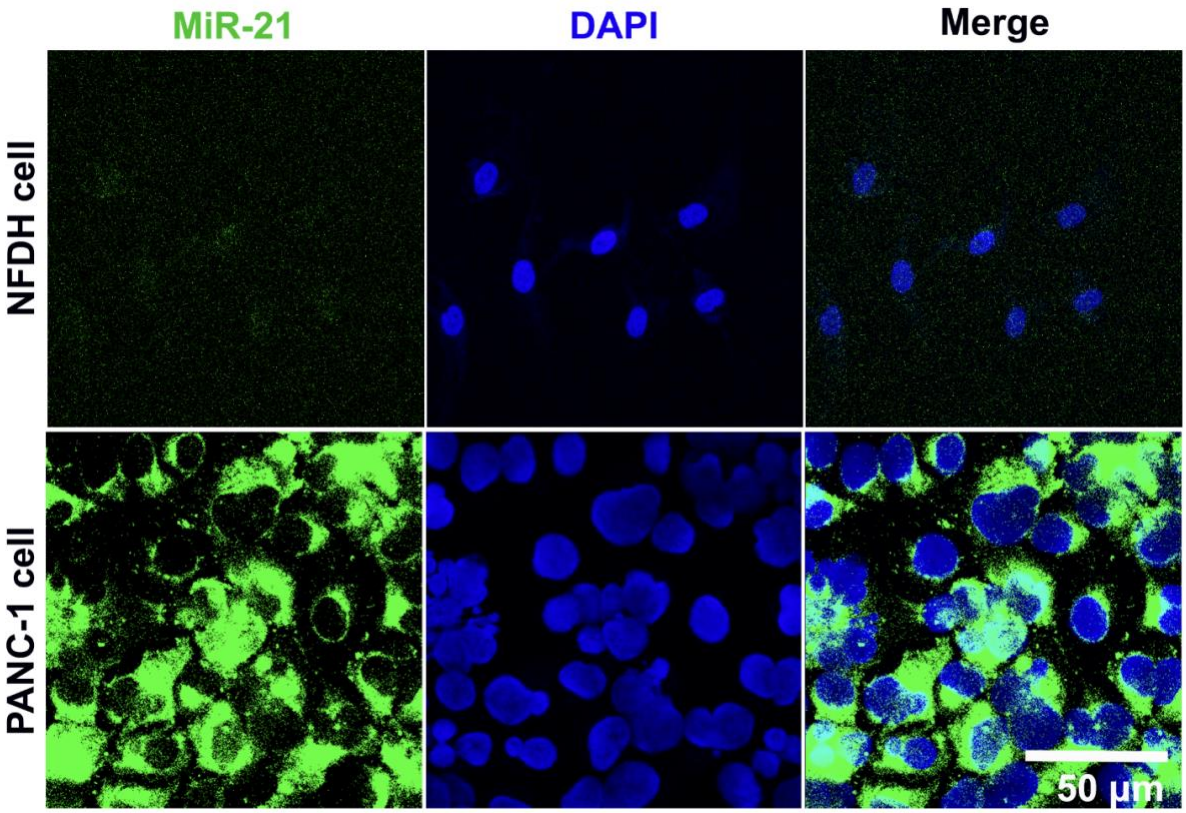

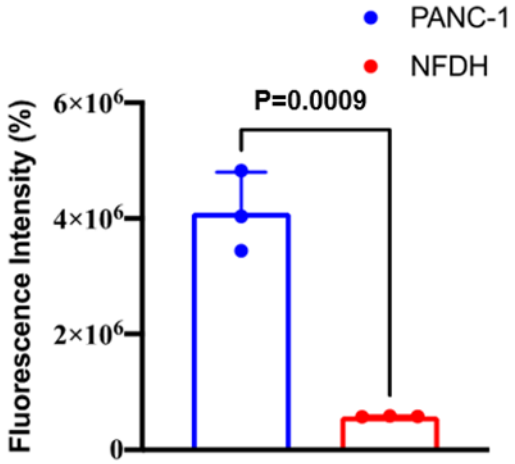

Supplementary Figure 13. The FISH method was first utilized to compare the miRNA-21 content between NFDH cells and PANC-1 cells. (n = 3 independent experiment, with similar results and the data are presented as mean values ± SD) All statistics were calculated using two-tailed paired t-test. Source data are provided as a Source Data file.

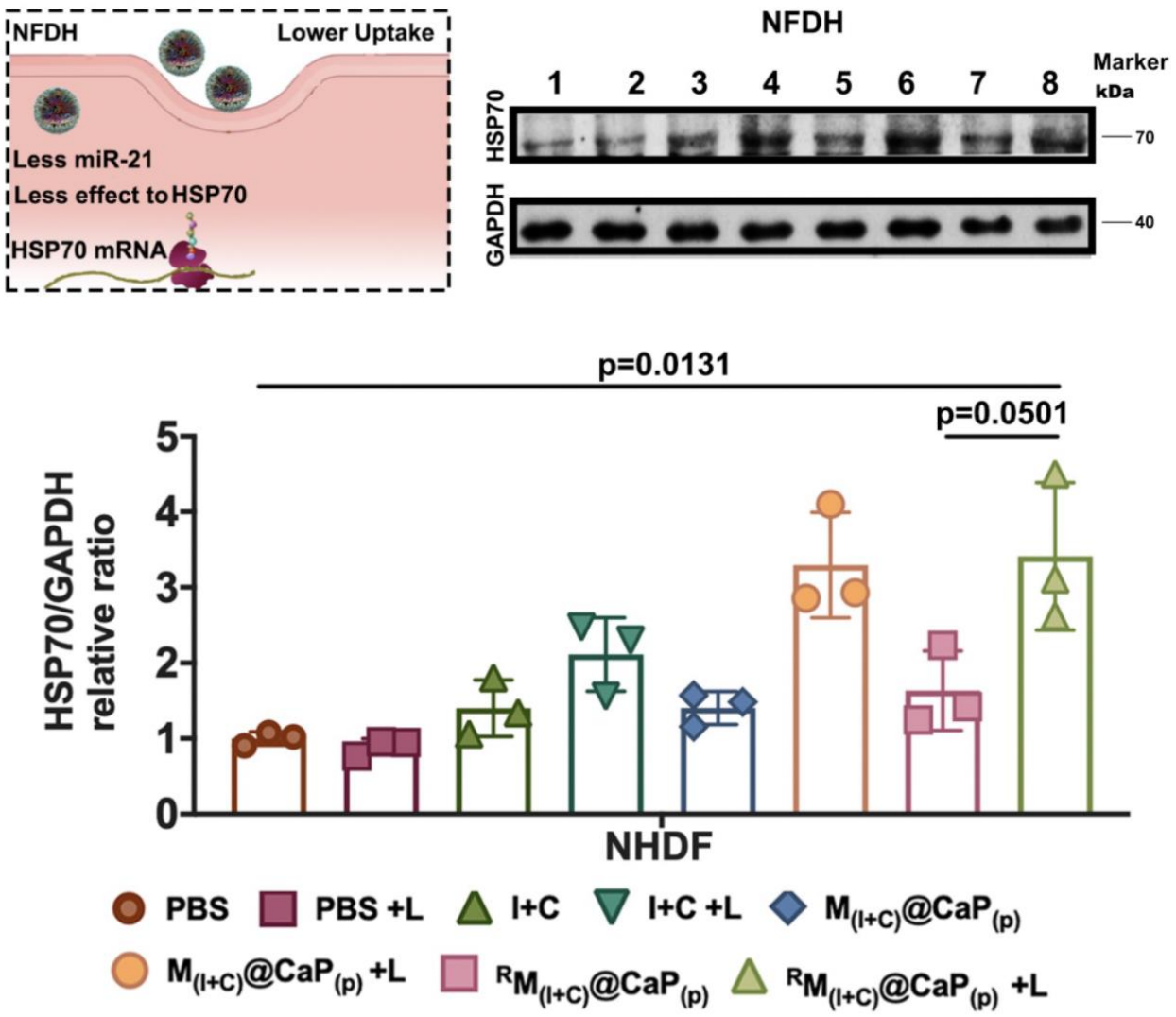

Supplementary Figure 14. Western blot results to test the generation of HSP70 in NFDH cells. (n = 3 independent experiments, with similar results) and the data are presented as mean values ± SD) All statistics were calculated using two-tailed paired t-test. Source data are provided as a Source Data file.

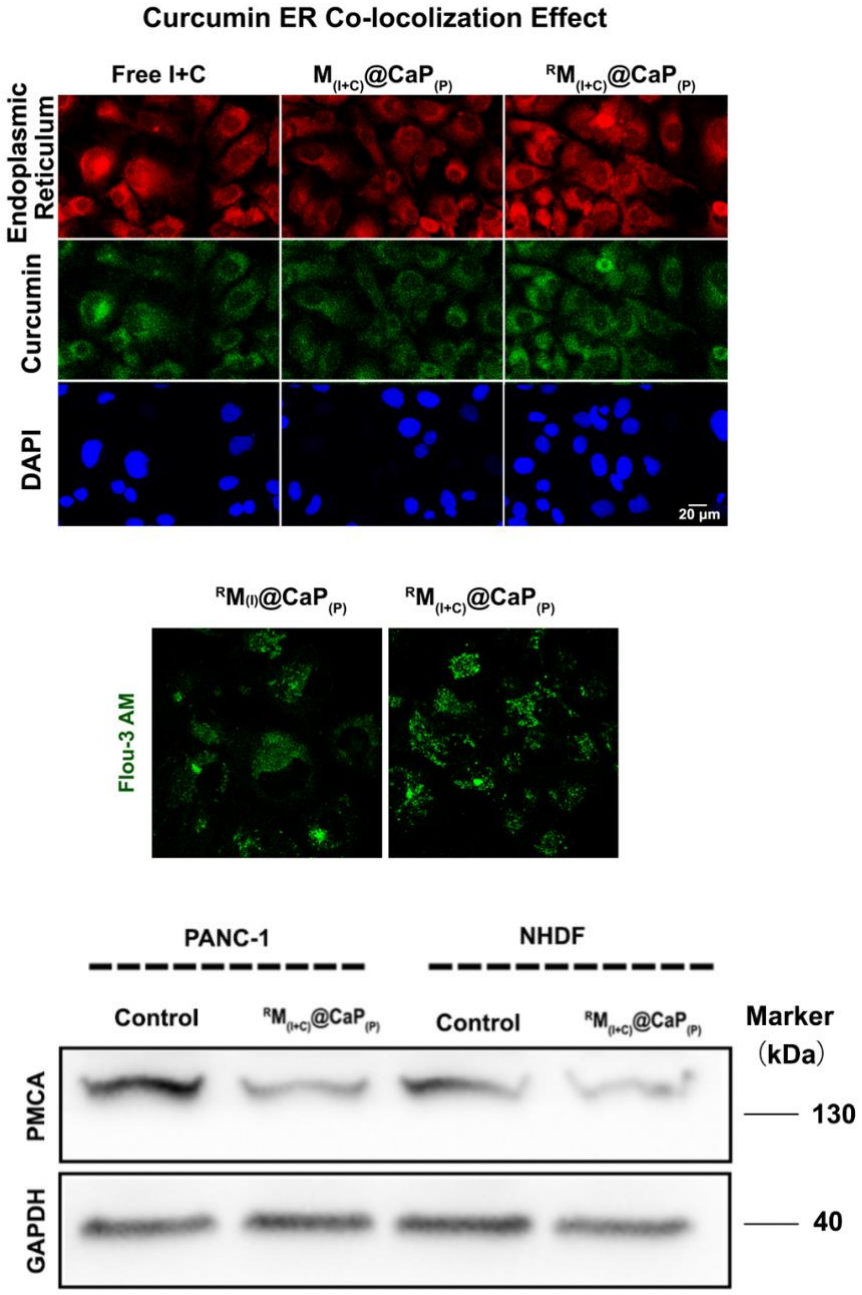

Supplementary Figure 15. Ca^{2+} levels detection and the WB results for plasma membrane calcium ATPase (PMCA) in NHDF and PANC-1 cells. With the assistance of curcumin, $^{R}M_{(I+C)}@CaP_{(p)}$ group showed higher Ca^{2+} levels compared with the group without Cur. The plasma membrane calcium ATPase (PMCA) in NHDF and PANC-1 cells are also tested through western blot. (n = 3 independent experiments, with similar results) Source data are provided as a Source Data file.

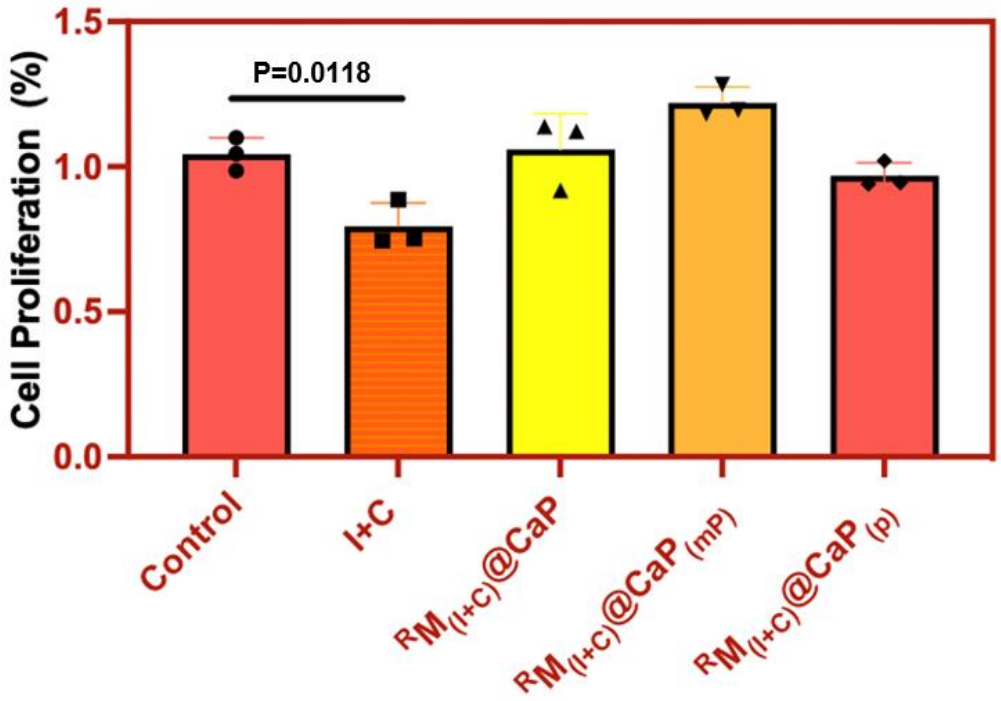

Supplementary Figure 16. WST-1 for NHDF cell lines. All groups were under laser irradiation. (n = 3 independent experiments and the data are presented as mean values ± SD) All statistics were calculated using two-tailed paired t-test. Source data are provided as a Source Data file.

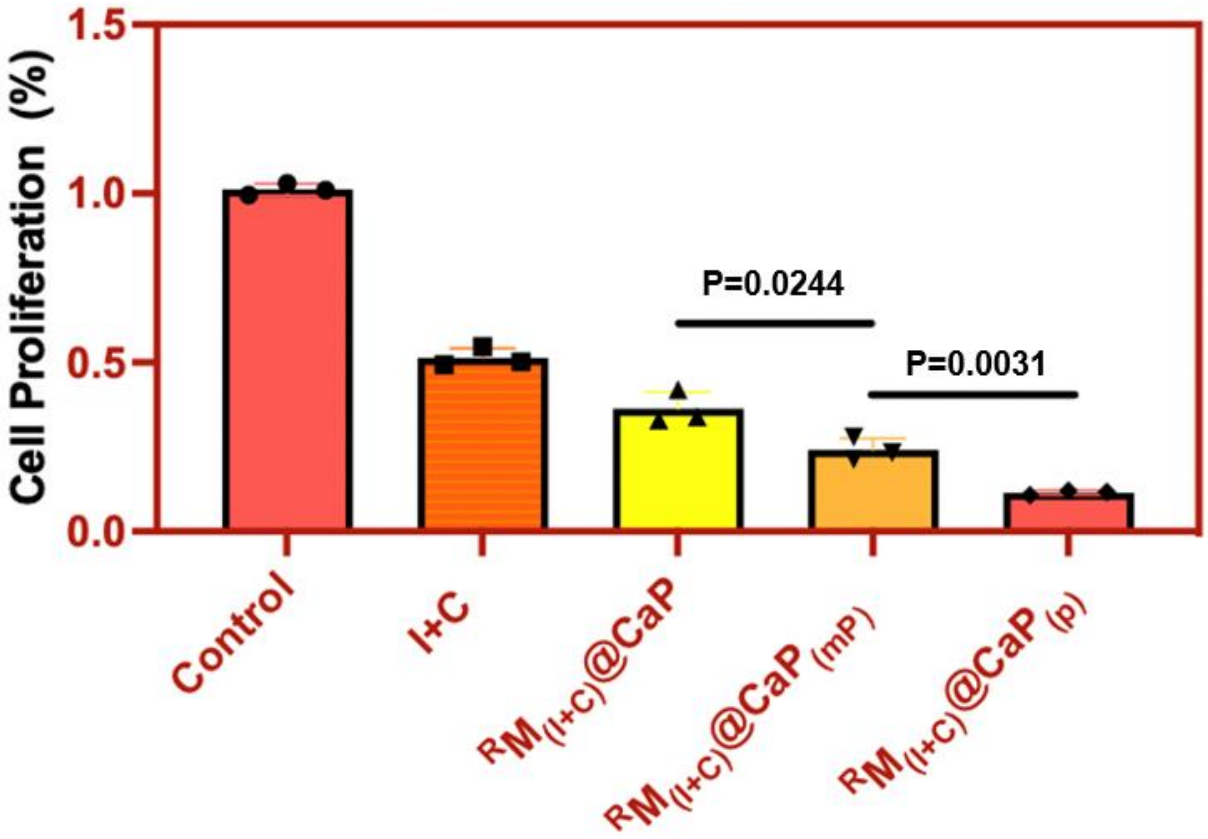

Supplementary Figure 17. WST-1 for PANC-1 cell lines. All groups were under laser irradiation. (n = 3 independent experiments and the data are presented as mean values ± SD) All statistics were calculated using two-tailed paired t-test. Source data are provided as a Source Data file.

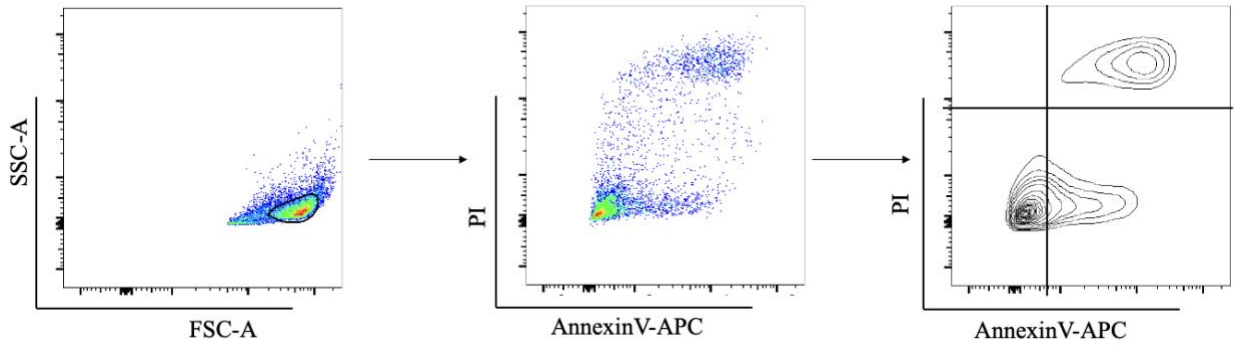

Supplementary Figure 18. Gating strategy for analyzing the cell apoptosis. (Account for Figure 7)

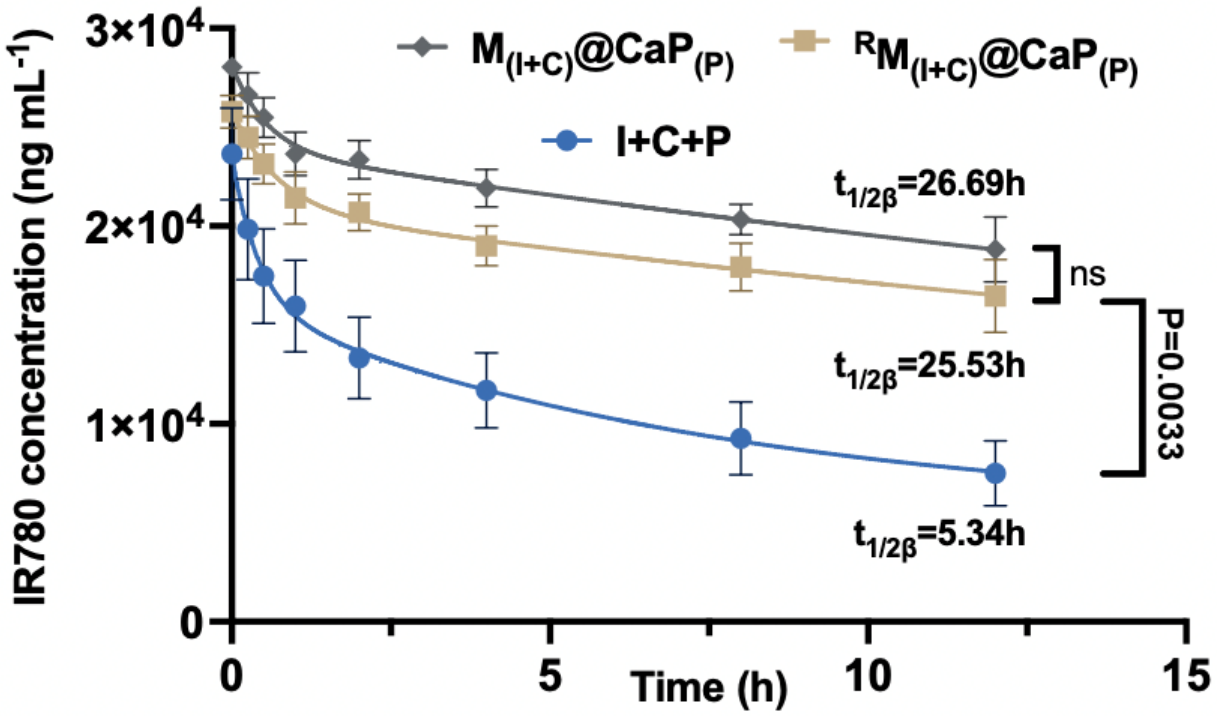

Supplementary Figure 19. Blood circulation and the blood half-life of the nanomachine. Blood circulation and the blood half-life of the nanomachine were investigated first to determine its pharmacokinetics and potential efficacy *in vivo*. (n = 3 independent experiments and the data are presented as mean values ± SD) All statistics were calculated using two-tailed paired t-test. Source data are provided as a Source Data file.

a

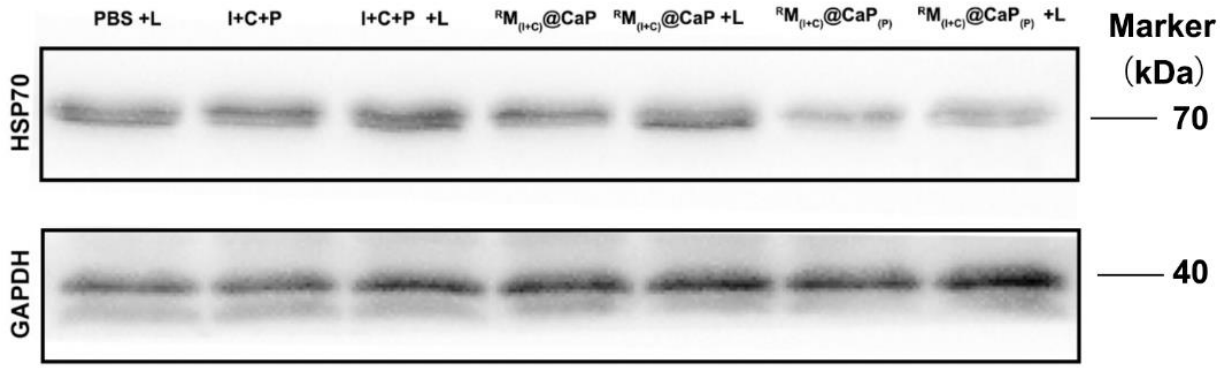

b

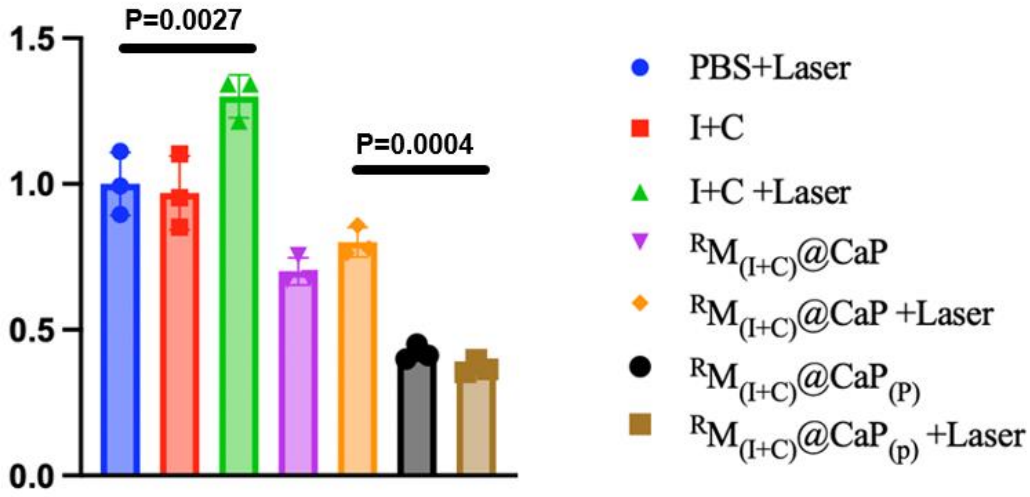

Supplementary Figure 20. In vivo western bolt for the HSP70 protein expression. (a) WB representative picture. (n = 3 independent experiments, with similar results) (b) Quantitively analysis by ImageJ. (n = 3 independent experiments and the data are presented as mean values ± SD) All statistics were calculated using two-tailed paired t-test. Source data are provided as a Source Data file.

The results demonstrate that in the pure drug I+C+P group, after being irradiated by the laser, the high temperature effectively activates HSP70, leading to upregulation of HSP70 expression compared to the PBS group. In contrast, for the formulation group without MNAzymes, we found that calcium phosphate, due to its mineralization effect on mitochondria, leads to insufficient cellular energy and downregulation of HSP70. This is consistent with the previous immunofluorescence and cellular experiment results. Furthermore, when MNAzymes are loaded, the nanosystem can effectively achieve silencing of HSP70 with an efficiency of approximately 65%.